The Journal of Chemical Physics PERSPECTIVE pubs.aip.org/aip/jcp

How the choice of exchange–correlation functional affects DFT-based simulations of the hydrated electron

Cite as: J. Chem. Phys. 162, 110901 (2025); doi: 10.1063/5.0253369
Submitted: 16 December 2024 • Accepted: 22 January 2025 •
Published Online: 19 March 2025

William R. Borrelli, Xiaoyan Liu, and Benjamin J. Schwartz[a]

AFFILIATIONS

Department of Chemistry and Biochemistry, University of California, Los Angeles, Los Angeles, California 90095-1569, USA

[a]Author to whom correspondence should be addressed: schwartz@chem.ucla.edu

ABSTRACT

Hydrated electrons are anionic species that are formed when an excess electron is introduced into liquid water. Building an understanding of how hydrated electrons behave in solution has been a long-standing effort of simulation methods, of which density functional theory (DFT) has come to the fore in recent years. The ability of DFT to model the reactive chemistry of hydrated electrons is an attractive advantage over semi-classical methodologies; however, relatively few density functional approximations (DFAs) have been used for the hydrated electron simulations presented in the literature. Here, we simulate hydrated electron systems using a series of exchange–correlation (XC) functionals spanning Jacob's ladder. We calculate a variety of experimental and other observables of the hydrated electron and compare the XC functional dependence for each quantity. We find that the formation of a stable localized hydrated electron is not necessarily limited to hybrid XC functionals and that some hybrid functionals produce delocalized hydrated electrons or electrons that react with the surrounding water at an unphysically fast rate. We further characterize how different DFAs impact the solvent structure and predicted spectroscopy of the hydrated electron, considering several methods for calculating the hydrated electron's absorption spectrum for the best comparison between structures generated using different density functionals. None of the dozen or so DFAs that we investigated are able to correctly predict the hydrated electron's spectroscopy, vertical detachment energy, or molar solvation volume.

I. INTRODUCTION

An excess electron in liquid water is known to form a stable, solvated species called the hydrated electron (e^-_{hyd}). Despite their apparent chemical simplicity, hydrated electrons have long been of interest due to their array of interesting properties and reactivity. With implications in fields ranging from radiation chemistry,[1–4] organic chemistry, and biochemistry,[4,5] understanding the nature and reactivity of hydrated electrons has been and continues to be an active area of research. Hydrated electrons are the simplest stable anion in solution, serve as strong reducing agents,[6–11] and are capable of reacting not only with organic molecules[6,8,12] but also with themselves.[3,8,9] They can be probed experimentally from the earliest stages of their formation up to their annihilation with ultrafast spectroscopic techniques,[13–15] and they are readily simulated via a variety of methodologies and levels of theory.

Interestingly, the rates of reactions involving hydrated electrons do not follow the Marcus theory of electron transfer,[16] meaning that the local solvent structure/reorganization of e^-_{hyd}'s must be different from those of other solutes that commonly undergo charge transfer reactions. For this reason, among others, there has been great interest in developing an understanding of the hydrated electron's solvation structure from simulations and experiments. Unfortunately, many experimentally observable quantities for this species only indirectly relate to the solvation structure. For example, the absorption spectrum is directly related to the size (radius of gyration) of the hydrated electron,[4,17] but this means that any simulation model that produces an electron with approximately the correct size will give a reasonable prediction of the spectrum. Observables that are more directly related to the local arrangement of water molecules around the electron include the partial molar volume (V_M), which is connected to the electron–water radial distribution function (RDF),[18] and ion-pairing behavior,[19–22] which involves the interaction of the e^-_{hyd}'s and ion solvation shells and the kosmotropic or chaotropic character of the ions involved.[23]

The inability of experimental methods to give a definitive measure of the solvation structure has inspired researchers to rely on simulation methods to build an atomistic picture of how water molecules orient around and behave near this object. However, different simulations yield different structures, and the debate as to the nature of the true solvation structure of the hydrated electron is hotly contested and ongoing.[4,19,24–29]

The earliest hydrated electron simulations were performed with mixed quantum–classical (MQC) molecular dynamics (MD),[30–34] allowing hundreds to thousands of solvent molecules to be treated classically, while the single excess electron is treated quantum mechanically by solving the Schrödinger equation for a single electron.[35] The interaction between the classical and quantum subsystems is accounted for via a one-electron pseudopotential, which is a parameterized potential function derived from *ab initio* theory molecular orbitals.[36] Many different electron–water pseudopotentials have been proposed to simulate the hydrated electron,[30–33] and each produces a different eigenvalue, radius of gyration, and solvation structure, as well as different predicted experimental observables.[18,30–33] Most such models predict that the electron density resides in a cavity from which water molecules are excluded, but details concerning the precise cavity size, fluctuations of the water around the cavity, the amount by which the electron density overlaps with the surrounding water, and the degree of orientational ordering of the first-shell water molecules all differ between models. Each model also predicts a different absorption spectrum for this object, none of which quantitatively matches experiment.[30–33] There is also mixed agreement between MQC models and experiment in modeling the temperature-dependent shift of the e^-_{hyd} absorption spectrum,[37,38] time-resolved photoelectron spectroscopy,[39] and V_M,[18] with no one model able to match experiment for all of these quantities.

More recently, improvements in computational resources have allowed *ab initio* methods to become tractable for condensed-phase systems such as the e^-_{hyd}. Currently, density functional theory (DFT) is the highest level of theory available to simulate reasonably large hydrated electron systems (up to 128 water molecules to date) on picosecond timescales. There has also been work using a multi-time step integrator to try to achieve MP2 level accuracy, although the system size was limited to only 47 waters with only a few-ps simulated trajectory.[40] Recently, a message-passing neural network architecture based on the deep potential framework[41] has been trained on PBEh DFT, allowing simulations of a DFT-based e^-_{hyd} with 128 and 256 water molecules. Despite this promise, the computational expense for pure DFT-based simulations is still an issue that significantly limits both system sizes and trajectory lengths (which also poses an obstacle to generating training data for machine-learned interatomic potentials).

One of the main issues with DFT is that it is known to be plagued by self-interaction errors (SIEs), which are particularly troublesome for simulating objects such as the e^-_{hyd}.[42] SIE also has a large impact on DFT-predicted bandgaps and reaction barrier heights[42] and varies greatly depending on the density functional approximation (DFA) being used: lower level exchange–correlation (XC) functionals, particularly those that do not include exact Hartree Fock (H–F) exchange, are particularly prone to SIEs. In combination with inadequate handling of dispersion interactions, SIE also has significant implications for the DFT-based modeling of the structure and dynamics of liquid water.[43] Clearly, having an inaccurate description of liquid water provides a difficult starting point for simulations of the hydrated electron, as the DFA must handle both the interactions between water molecules and describe the excess electron, which is located primarily in between the water molecules.

This leaves simulators with a set of questions to answer when choosing to simulate hydrated electron systems with DFT: What system size is necessary to converge the properties of interest? Which XC functional best balances computational cost and accuracy (or happens to give the best cancellation of errors[43]), particularly given that DFT is not a systematically improvable theory? If a hybrid functional is used, what percent of exact exchange is the most optimal (as is particularly pertinent for predicting the correct bandgap of bulk water[44])? Here, we present a series of DFT-based simulations of the e^-_{hyd} with a range of DFAs in order to shed light on how different choices alter the simulated structure, dynamics, and experimentally observable properties. We climb "Jacob's Ladder"[45] from the local density approximation (LDA) up to the hybrid meta-generalized gradient approximation (meta-GGA) in order to better understand the XC functional dependence of hydrated electron simulations. Table I shows the XC functionals as well as two MQC models that we included in this analysis, where the number in parentheses indicates the amount of exact Hartree–Fock exchange used (where applicable). Our analysis includes several non-hybrid and hybrid functionals with different amounts of exact exchange to allow an investigation into the role of exact exchange in the simulated properties of the e^-_{hyd}.

To date, the majority of DFT-based hydrated electron simulations have used a hybrid GGA functional, PBEh, with very little work

TABLE I. DFT-based and MQC pseudopotential models of the hydrated electron investigated in this work, including whether the DFA includes H–F exchange (hybrid or not) and, if so, the amount (percentage in parentheses). One-electron pseudopotential-based MQC models are listed in bold text.

DFAs/MQC models tested		
XC DFA	Hybrid	Functional/**Model**
LDA	No	LDA
	Yes	LDAh(25%)
GGA	No	PBE
	Yes	PBEh(25%)
	Yes	PBEh(40%)
MGGA	Yes	R2SCANh(25%)
	Yes	R2SCANh(50%)
	No	REVTM
	No	SCAN
	Yes	SCANh(10%)
	Yes	SCANh(25%)
	No	R2SCAN
MQC	No	**TB**
	No	**TBOpt**

exploring either the amount of H–F exchange or DFAs from different rungs of Jacob's ladder.[45] In this work, we show that improving DFT-based simulations of the e^-_{hyd} is not as simple as moving up Jacob's Ladder,[45] as the predicted properties of hydrated electrons (including whether or not they even exist) do not monotonically improve with the complexity of the chosen XC functional. For each DFA, we calculate a series of solvent structural and charge density shape parameters, as well as e^-_{hyd} electronic structure measures, to explore how sensitive electron–solvent interactions are to the choice of the DFA. We find that some DFAs produce hydrated electrons that remain delocalized throughout the simulation cell or react with water at a rate orders of magnitude too high, while others produce a cavity-localized e^-_{hyd}; there is no obvious way to determine *a priori* which DFAs will produce which behavior. Moreover, among XC functionals that produce a localized e^-_{hyd}, we find that the equilibrium structure of the waters around the electron is not qualitatively all that different, even for very simple functionals such as LDA.

We also work to highlight the challenges faced in calculating the absorption spectrum of DFT-simulated hydrated electrons by exploring two different methods for obtaining the spectrum: periodic Tamm–Dancoff Approximation time-dependent DFT (TDA TD-DFT) and non-periodic time-dependent DFT (TD-DFT) with unit cell replication and an optimally-tuned range-separated hybrid functional.[15] We find that the use of periodic TDA TD-DFT produces a severe blueshift in the calculated absorption spectra for every DFA we explored and that this blueshift is made even worse with increasing amounts of H–F exchange. However, the blueshift can be largely alleviated by using the non-periodic TD-DFT methodology, although none of the DFAs we tested predict spectra that are close to being in agreement with experiment. Overall, we conclude that no matter what XC functional is used, at currently accessible simulation sizes and trajectory lengths, DFT does not provide an experimentally faithful description of the hydrated electron.

II. METHODS

A. Molecular dynamics propagation

All *ab initio* DFT calculations were done using the CP2K[46] software package. Initial atomic configurations for an excess electron in a box of 64 quantum mechanical waters were taken from our previous studies[24,25,29] using the PBEh functional with 25% exact exchange and Grimme's D3 dispersion correction.[47] This provides for the presence of a stable trap into which the excess electron could localize immediately. Since we have previously shown that hydrated electrons (including those simulated by DFT)[48] are trap-seeking rather than trap-digging,[49] starting from a pre-existing cavity maximizes the amount of equilibrated simulation data. Although we have previously argued that a box of 64 water molecules is too small to eliminate finite-size effects for simulating the e^-_{hyd},[25,29] we use this system size both to compare with the vast majority of results in the literature, which were run at this size, and to allow reasonably long trajectory lengths for each functional we tested.

For the different DFT-based simulations, a grid cutoff of 500, 700, 500, 1200, 1000, 700, and 1000 Ry was used for the LDA, LDAh, PBEh, SCAN, R2SCAN, REVTM, and R2SCANh simulations, respectively. Core electrons were treated using Goedecker–Teter–Hutter (GTH) pseudopotentials,[50] optimized for each chosen functional [i.e., GTH-LDA, GTH-SCAN, GTH-PBE, etc.]. The TZVP-GTH triple-zeta basis set was used for all calculations, and H–F calculations were expedited with the auxiliary density matrix method (ADMM)[51] method using the cFIT3 basis set.[51] All simulations were run with a 0.5-fs time step in the N, V, T ensemble with a Nosé–Hoover[52] chain thermostat to maintain a constant temperature of 298 K. We note that D3 was used for the PBEh(25% and 40%) simulations but was not used for the other functionals we investigated. The PBEh-based simulations used a simulation cell length of 12.519 Å, while all other simulations used a 12.427 Å length. DFAs that produced a localized hydrated electron were propagated long enough to provide several ps of equilibrated data for analysis. Simulations were propagated for 30, 4.5, 20, 6, 3.5, and 3.2 ps for the LDA, LDAh(25%), PBEh(25%), PBEh(40%), R2SCANh(25%), and R2SCANh(50%) DFAs, respectively.

B. Calculation of R_g and solvent structure measures

The center of mass (com) and radius of gyration (R_g) of the hydrated electron for each trajectory were calculated using an in-house Python script directly from the atomic position files and spin density cube files generated by CP2K.[46] Radial distribution functions (RDFs) were calculated from the electron's center of mass to the positions of the water oxygen atoms. We define the cavity region associated with the e^-_{hyd} as the region from $r = 0$ to where the RDF first reaches a value of 1. Solvent shells are defined as lying between the minima of the RDF.

First-shell water angular distributions were calculated using an in-house Mathematica script. This calculation involves taking the dot product between two unit vectors involving the first-shell water molecules, defined as those inside the location of the first minimum in the RDF. The first unit vector begins at the electron's center of mass and points to the oxygen atom of a first-shell water molecule,

$$\hat{r}_{e^-_{hyd}-O,i} = \frac{\vec{r}_{O,i} - \vec{r}_{e^-_{hyd}}}{|\vec{r}_{O,i} - \vec{r}_{e^-_{hyd}}|}, \quad (1)$$

where $\vec{r}_{O,i}$ is the position of oxygen atom i in the first shell of the e^-_{hyd} and $\vec{r}_{e^-_{hyd}}$ is the position of the center of mass of the hydrated electron. The second unit vector begins at the oxygen atom of the first-shell water molecule and points toward the midpoint between the two hydrogen atoms bonded to that oxygen atom (i.e., along the water dipole vector),

$$\hat{r}_{H_m-O,i} = \frac{\vec{r}_{H_m,i} - \vec{r}_{O,i}}{|\vec{r}_{H_m,i} - \vec{r}_{O,i}|}, \quad (2)$$

where $\vec{r}_{H_m,i}$ is the position of the midpoint between the two hydrogen atoms bonded to oxygen atom i. With this definition, first-shell waters that have their dipole pointing directly toward the hydrated electron's center have a dot product of −1.0, waters that point their O atoms toward the electron have a dot product of +1.0, and waters that point an O–H bond directly toward the electron's center give a dot product of ~ −0.7.

We examine how cavity-like a given hydrated electron's solvation structure is by using an order parameter called q_{cav}, which we have presented in a previous study.[53] This measure effectively counts the number of waters "inside" the hydrated electron, such that q_{cav} values near unity indicate a non-cavity hydrated electron, while values approaching 0 indicate a more traditional cavity hydrated electron. This measure is calculated as follows:

$$q_{\text{cav}} = \sum_{i=1}^{N} S(|\mathbf{R}^i - \vec{r}_{e^-_{\text{hyd}}}|), \tag{3}$$

where the smoothing function $S(r)$ is defined as

$$S(r) = \frac{1}{\exp\left[\kappa(r - r_c)\right] + 1}, \tag{4}$$

where $\mathbf{R}^i$ is the distance of the ith water molecule's oxygen atom from the e^-_{hyd} center of mass. The smoothing function $S(r)$ defines the region over which we count water molecules, taken to be 1.75 Å from the electron's center. The value of κ, which modulates how abruptly the cutoff distance tapers from the electron's center, was set to be 10 Å^{-1}.

To characterize the shape of the e^-_{hyd}, we calculate the asphericity, A, which we also have used in a previous study.[53] The asphericity is a measure that is derived from diagonalizing the inertia tensor of the hydrated electron's charge density, where the resulting eigenvalues determine A as

$$\langle A \rangle = \frac{\langle \text{Tr}^3 - 3M \rangle}{\langle \text{Tr}^2 \rangle}, \tag{5}$$

in which Tr indicates the trace of the eigenvalues and M is the sum of the three minors. With this definition, a perfectly spherical charge distribution yields $A = 0$, while an infinitely thin needle would give $A = 1$.

C. Periodic Tamm–Dancoff approximation TD-DFT spectra calculations

Fully-periodic TDA TD-DFT calculations of the hydrated electron's absorption spectrum were done in CP2K.[46,54] Atomic configurations were sampled from our *ab initio* molecular dynamics (AIMD) runs and used as inputs in a series of single-point excited-state calculations. For each functional, the grid cutoff, basis set, and pseudopotential parameters were used as listed above to calculate ten excited states. Absorption spectra were generated from the TDA TD-DFT excited states by binning the excitation energies relative to the ground state ($\Delta E_{0,i}$), weighted by their oscillator strengths ($\mu_{0,i}$),

$$I(E) = \left\langle \sum_{i=1}^{N} |\mu_{0,i}|^2 \Delta E_{0,i} \sqrt{\alpha/\pi} \exp\left(-\alpha(E - \Delta E_{0,i})^2\right) \right\rangle, \tag{6}$$

where the angle brackets refer to an ensemble average over uncorrelated configurations. We then convoluted each bin with a Gaussian kernel in order to generate a broadened spectrum.

D. Non-periodic TD-DFT spectra calculations

Non-periodic TD-DFT calculations were done in Q-Chem,[55] using the LRC-ωPBE functional and the 6-31++G* basis set, following the procedure outlined in Ref. 15. The position of the excess electron was centered in our simulation cell of 64 fully quantum-mechanical water molecules. Twenty-six periodically replicated simulation cells containing simple point charges at the positions of the replicated water molecules were added around the main cell to prevent the excess electron from spilling out into the vacuum beyond the explicit simulation box. In our previous study,[25] we determined that the optimized ω value to satisfy Janak's theorem for hydrated electron configurations generated from the PBEh functional with 25% H–F exchange was ω = 175 a_0^{-1}, and we used this optimized value for configurations generated from all of the DFAs we tested so that the resulting spectra could be compared at the same level of theory.

E. Finite size effects

As discussed throughout this work, none of the DFAs we tested yield results that are in agreement with experiment for most properties of the hydrated electron. It is possible that increasing the number of quantum mechanical waters (to ≫64) in DFT-based e^-_{hyd} simulations could bring these predictions into better agreement with experiment, but such large system sizes are currently computationally intractable. Our group has explored finite size effects for various properties of the hydrated electron simulated using the PBEh functional with 25% exact exchange.[25,29] We found that measures such as radial and angular distribution functions, the radius of gyration, and the absorption spectrum were not especially sensitive to the simulated system size between 47 and 128 waters.[25] The partial molar volume of the hydrated electron does show moderate finite size effects, and we found that this quantity is significantly underestimated for system sizes up to 128 waters.[29] The vertical binding energy (VBE) of the e^-_{hyd} is also moderately impacted by finite size effects. Interestingly, a linear extrapolation to infinite system size brings both the VBE and V_{M} into agreement with experimental values, although we have argued that this correspondence is likely coincidental due to the relatively large slopes of the linear fits and the fact that the simulated solvation structure does not change in any systematic way.[25,29] Based on the fact that these previous studies showed only modest finite size effects, we expect that such effects are likely not to play an important role for the DFAs explored in this work. In terms of comparing the properties of the e^-_{hyd} simulated with different DFAs, we note that, here, we test each DFA at the same system size so that whatever finite size effects do exist are at least similar across the different DFAs.

III. RESULTS AND DISCUSSION

A. Localization and radius of gyration (R_g)

We begin our analysis by examining the size of the e^-_{hyd} simulated with different DFT XC functionals. Figure 1 shows the difference between the simulated R_g for each functional and the room-temperature experimental value of 2.45 Å,[17] while Table II presents the raw R_g values for each DFA. Out of the 12 exchange–correlation functionals that we tested, only six produced stable localized hydrated electrons. For most of the non-hybrid DFAs that we studied (PBE, REVTM, SCAN, and R2SCAN), the electron remained delocalized across the entire simulation cell (R_g roughly equal to 6 Å, which is half the simulation box length), even in the presence of a pre-existing cavity trap. This delocalization is unphysical, given that spectral moment analysis clearly shows that the electron is localized.[17] Interestingly, the LDA functional, which is nominally the simplest non-hybrid DFA, actually produces a localized, stable hydrated electron, with an average R_g of ~2.7 Å, in rough agreement with experiment. In contrast, the SCANh hybrid DFA, depending on the percentage of H–F exchange used, either produces a delocalized e^-_{hyd} or has the electron react with the surrounding water, abstracting a proton to produce a H atom and a

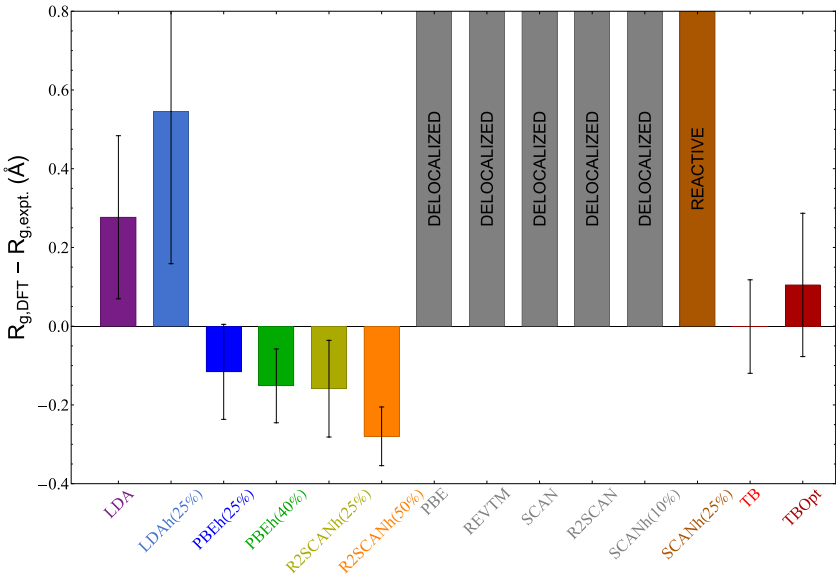

FIG. 1. Difference between the average e^-_{hyd} radius of gyration simulated with different DFAs and the experimental value of 2.45 Å.[17] We see that all the non-hybrid functionals, except LDA, produce delocalized hydrated electrons. With the exception of SCANh (which is spuriously over-reactive for 25% H–F exchange and delocalized for 10% H–F exchange),[56] the other hybrid functionals we examined produce localized hydrated electrons. The LDA-based DFAs over-estimate the experimental value, while the R2SCANh functionals under-estimate it. PBEh gives an R_g value that is within the error of experiment. The error bars represent one standard deviation across MD snapshots.

TABLE II. e^-_{hyd} size and shape descriptors, including the radius of gyration, asphericity, and q_{cav} measures. The radii of gyration for the LDA-based functionals are slightly over-estimated relative to experiment, while the hybrid GGA and hybrid meta-GGAs all produce hydrated electron R_g's that are slightly under-estimated or within the error of experiment. The asphericity measures how non-spherical the e^-_{hyd} is, and all the DFAs we tested that produced localized hydrated electrons had quite spherical charge densities with little shape fluctuation. The q_{cav} measure integrates the number of water molecules embedded within the electron's charge density. Most of the DFAs that produced localized e^-_{hyd}'s (except LDAh(25%) show relatively hard cavities. All uncertainties are standard deviations. Uncertainties for the partial molar volume were computed as the standard deviation of V_M values obtained from the RDFs of individual simulation snapshots.

e^-_{hyd} size and shape descriptors					
Functional	R_g (Å)	Asphericity	q_{cav}	VBE (eV)	V_M (cm^3/mol)
LDA	2.73 ± 0.21	0.0012 ± 0.0006	0.34 ± 0.22	1.86 ± 0.33	4.5 ± 2.3
LDAh(25%)	3.0 ± 0.4	0.0039 ± 0.0013	0.73 ± 0.35	1.45 ± 0.27	2.90 ± 3.0
PBE	Delocalized	⋯	⋯	⋯	⋯
PBEh(25%)	2.33 ± 0.12	0.0014 ± 0.0009	0.23 ± 0.24	2.14 ± 0.36	8.0 ± 3.1
PBEh(40%)	2.30 ± 0.10	0.0013 ± 0.0007	0.15 ± 0.16	1.78 ± 0.26	8.3 ± 2.9
R2SCANh(25%)	2.29 ± 0.12	0.0012 ± 0.0007	0.26 ± 0.20	1.94 ± 0.46	3.5 ± 2.8
R2SCANh(50%)	2.17 ± 0.07	0.0012 ± 0.0007	0.14 ± 0.11	2.10 ± 0.20	4.3 ± 3.3
REVTM	Delocalized	⋯	⋯	⋯	⋯
SCAN	Delocalized	⋯	⋯	⋯	⋯
SCANh(10%)	Delocalized	⋯	⋯	⋯	⋯
SCANh(25%)	Reactive	⋯	⋯	⋯	⋯
R2SCAN	Delocalized	⋯	⋯	⋯	⋯
TB	2.45 ± 0.12	0.0028 ± 0.0019	0.012 ± 0.066	⋯	23[18]
TBOpt	2.55 ± 0.18	0.0027 ± 0.0018	0.41 ± 0.42	⋯	11[33]
Expt.	2.45	⋯	⋯	3.5	26 ± 6

hydroxide ion. Although hydrated electrons are known to react with water in this way, we showed in a previous study that the e^-_{hyd} simulated with SCANh(25%) underwent this reaction at a rate ~12 orders of magnitude faster than in experiment.[56]

The fact that not all hybrid functionals produce localized electrons and not all non-hybrid functionals produce delocalized electrons shows clearly that DFT is not a systematically improvable level of theory with respect to the choice of the DFA.

The formation of a stable and localized e^-_{hyd} likely depends on a careful balancing of interrelated factors, such as the magnitude of SIE and a particular DFA's prediction of the bulk water bandgap, water hydrogen bond strength, and water translational and rotational dynamics.

Overall, the XC functionals that yield a localized e^-_{hyd} predict the radius of gyration reasonably well, with the LDA-based functionals being slightly too large and the meta-GGA hybrid functionals being slightly too small. These results make sense given the dependence of R_g on the self-interaction error of the functional, as well as the predicted bandgap of water. Better handling of SIEs in the meta-GGA DFAs induces a more localized charge density, which lowers the R_g, while changes in the predicted water bandgap alter the amount of electron density donated into the anti-bonding orbitals of water molecules near the electron, which can greatly inflate R_g. Clearly, the LDA-based functionals have insufficient handling of SIEs while the hybrid GGAs and meta-GGAs either slightly underestimate the bandgap of liquid water or over-localize the density, given the amount of H–F exchange used.

B. Solvation structure of different simulation models of the hydrated electron

1. Hydrated electron–water radial distribution functions

To further investigate the electron–water structure from each of our DFT-based simulations, we examine electron–water radial distribution functions (RDFs) or $g(r)$'s. RDFs are based on the distances at which solvent molecules prefer to sit away from the e^-_{hyd}'s center and, thus, provide a readout of how strongly ordered the solvent is around the electron.

The upper panels of Fig. 2 show electron-oxygen RDFs for all the DFAs we tested that produced localized hydrated electrons, as well as for two well-studied one-electron pseudopotential MQC models of the e^-_{hyd} (the traditional cavity TB model[30] and the much softer cavity TBOpt model[31]). We can estimate the cavity size as the distance at which the electron–water oxygen $g(r)$ reaches a value of 1, and these values are tabulated in Table III along with other pertinent RDF distances. The two one-electron models produce e^-_{hyd}'s with cavities that show very little structuring of surrounding waters, meaning there are no distinct solvation shell peaks, and the RDF decays to unity at relatively small distances from the electron's center. All the DFT-based electron–water RDFs are highly structured [similar to past work with the PBEh(25%) and PBEh(40%) DFAs[25,28]], with the exception of LDAh(25%), which is less structured and more similar to TBOpt. Overall, despite modest changes in the cavity size and solvation shell peak heights and widths, the hydration structures of DFT-simulated hydrated electrons are quite similar for all the XC functionals we tested that produce localized e^-_{hyd}'s.

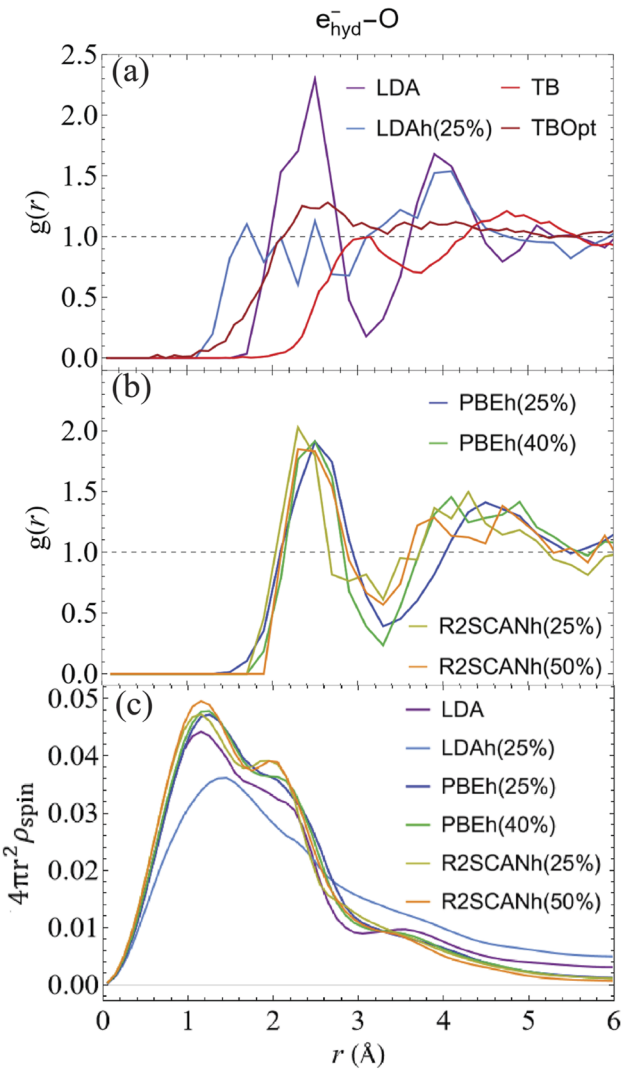

FIG. 2. (a) Electron-oxygen radial distribution functions (RDFs) produced by "lower level" DFAs [LDA: purple curve and LDAh(25%): blue curve], as well as the one-electron MQC models [TB (bright red curve) and TBOpt (maroon curve)]. The one-electron models and LDAh(25%) give much less structured RDFs than LDA. (b) Electron-oxygen RDFs for the "higher level" hybrid functionals (PBEh and R2SCANh), are very highly structured, similar to LDA. (c) Charge distributions for the excess electron (plotted as $4\pi r^2\rho$, where ρ is the spin density) for each DFA that produced a localized e^-_{hyd}. Each distribution has three peaks corresponding to charge density in the central cavity, on the first solvation shell waters, and between the first and second solvation shells. Increasing the amount of H–F exchange for the R2SCANh functional further localizes the density into the central cavity. Increasing H–F exchange by going from LDA to LDAh(25%), however, has the opposite effect, spreading the density out onto and well past the first-shell water molecules.

2. Hydrated electron solvation coordination numbers

In cavity-forming models of the e^-_{hyd}, the central cavity is solvated by a variable number of water molecules at any given instant. The average number of coordinating waters can be calculated either by integrating the RDF over the first solvent shell peak or by counting the number of waters within a first shell cutoff region of the electron cavity. On average, most models tend to produce a 3- to 5-coordinate species, with varying degrees of fluctuation in the number of first-shell waters. Table III gives the e^-_{hyd} oxygen and hydrogen coordination numbers (CNs) for each XC functional we tested; the details of the coordination number computation are given in Sec. II.

TABLE III. e^-_{hyd} solvation structure parameters, including important distances for features of the RDF as well as oxygen and hydrogen coordination numbers. Most of the RDF features are similar between the DFAs that produced localized e^-_{hyd}'s, although LDAh(25%) has a much smaller cavity region compared to the others. Electron–water first-shell coordination numbers are also similar in the range of 4–5 waters, although LDAh(25%) has only 2–3 first-shell waters.

e^-_{hyd} solvation structure descriptors					
Functional	r_{cav} H(O) (Å)	$r_{1^{st}\text{-shell}}$ H(O) (Å)	$r_{2^{nd}\text{-shell}}$ H(O) (Å)	O coord #	H coord #
LDA	0.85(1.96)	2.1(3.1)	3.7(4.7)	4.0 ± 0.17	3.95 ± 0.25
LDAh(25%)	0.32(1.6)	1.9(2.88)	4.5(5.5)	2.5 ± 0.7	2.2 ± 0.7
PBE	...	...	...	...	...
PBEh(25%)	0.97(2.1)	2.3(3.3)	4.3(5.5)	4.6 ± 0.6	4.4 ± 0.6
PBEh(40%)	1.0(2.13)	2.3(3.3)	4.65(5.7)	3.9 ± 0.4	3.8 ± 0.5
R2SCANh(25%)	0.92(2.02)	2.3(3.3)	5.1(5.7)	4.4 ± 0.8	4.1 ± 0.7
R2SCANh(50%)	1.04(2.1)	2.3(3.3)	5.3(5.7)	4.5 ± 0.6	4.2 ± 0.5
REVTM	...	...	...	...	...
SCAN	...	...	...	...	...
SCANh(10%)	...	...	...	...	...
SCANh(25%)	...	...	...	...	...
R2SCAN	...	...	...	...	...
TB	2.0(3.1)	2.7(3.7)	6.1(6.0)	4.2 ± 1.1	3.9 ± 1.1
TBOpt	1.17(2.1)	2.3(3.3)	4.5(5.3)	4.7 ± 11	3.8 ± 1.0

All the functionals/models that we tested that produced localized hydrated electrons resulted in coordination numbers between 3 and 5 waters with the exception of LDAh(25%), which had a much lower average coordination number of only 2-to-3 waters. The similarity between the oxygen and hydrogen coordination numbers for most DFAs suggests that first-shell waters in DFT-based simulations coordinate the e^-_{hyd} via a hydrogen-bonding motif, as we have documented previously for PBEh(25%).[24]

3. Hydrated spin density distributions

The degree to which charge density is donated onto surrounding water vs between the surrounding water molecules is a crucial property of e^-_{hyd} solvation. This is because significant electron density donation onto water can inflate the hydrated electron's radius of gyration, which, in turn, will alter both the predicted spectroscopy and the reactivity of the neighboring water molecules.[9,56] One can quantify how the hydrated electron's charge density is partitioned in its environment by plotting its spin density distribution, shown for each of the tested functionals that produce a localized e^-_{hyd} in Fig. 2(c). These distributions indicate the probability of finding part of the excess electron's charge as a function of distance r from the center of mass.

Figure 2(c) shows that each of the DFAs we tested that produce localized e^-_{hyd}'s has a charge distribution with three peaks, corresponding to (1) charge localized in the central cavity region, (2) charge residing on the first-shell waters, and (3) charge residing between the first- and second-shell waters. All the functionals, with the exception of LDAh(25%), show a cavity peak centered near 1.2 Å. R2SCANh(50%) gives the most prominent cavity peak, indicating that going from a GGA to a meta-GGA functional and/or increasing the amount of H–F exchange further localizes the charge density into the cavity. The LDA and LDAh(25%) DFAs yield more broad charge distributions compared to the GGA hybrids and meta-GGA hybrids that we tested, which is consistent with the expected increased self-interaction error for the LDA-family functionals. The fact that LDAh(25%) has a broader distribution than LDA provides an example of the unpredictable way in which introducing H–F exchange impacts the accuracy of a given functional.[44] In this case, even though adding H–F exchange relative to the pure LDA functional should improve SIEs, the description of the water bandgap likely worsens, leading to easier donation into the surrounding water LUMOs and, thus, a significant increase in the spatial extent of the e^-_{hyd}.

4. Hydrated electron asphericity and cavity parameters

Besides the radial extent of the charge distribution, one can also calculate how spherical the e^-_{hyd} is via the asphericity, A, defined in Sec. II. Small values of the asphericity indicate a more spherically symmetric charge density, while larger values indicate deviation from spherical symmetry. For the DFAs we tested that produced localized hydrated electrons, the charge distribution turns out to be quite spherical, as summarized in Table II, although LDAh(25%) shows deviations from spherical symmetry that are comparable to those seen with the one-electron TB and TBOpt MQC models.

To understand how "hard" of a cavity structure each DFA produces for the e^-_{hyd}, we computed a cavity parameter (q_{cav}, also defined in Sec. II), which effectively counts the number of waters that penetrate into the bulk of the electron's charge density. Most DFAs produce fairly hard cavities, giving q_{cav} values less than 0.30, as summarized in Table II. Interestingly, LDAh(25%) shows the softest cavity structure of all the models we examined. We note, however, that all the DFT simulations yield a much softer cavity than

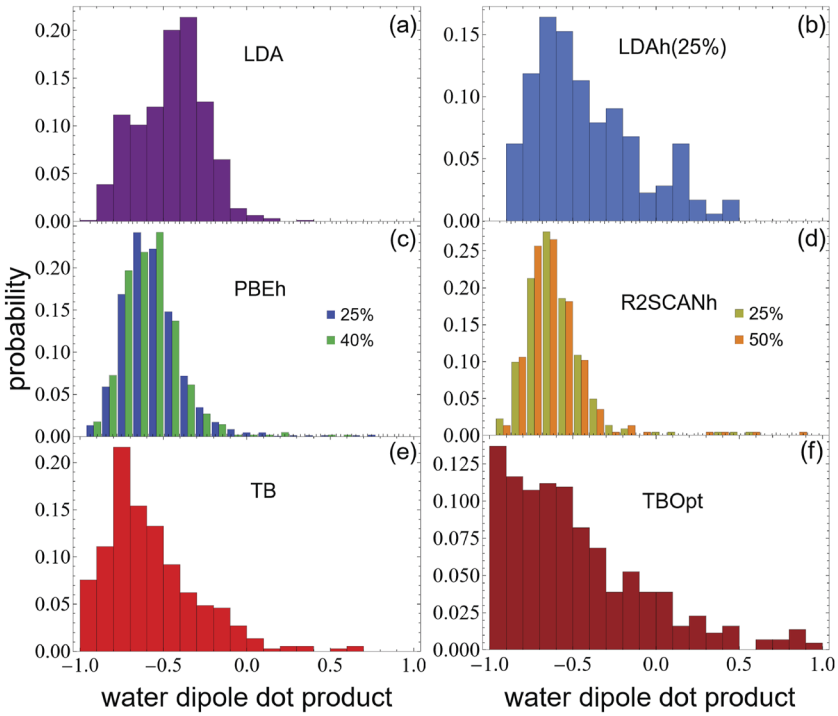

FIG. 3. Water dipole dot product (angular) distributions of first-shell water molecules around e^-_{hyd}'s simulated by DFT using DFAs that produced a localized species, as well as the TB and TBOpt pseudopotential models. For electrons simulated via DFT, the LDA and LDAh(25%) DFAs give less-structured angular distributions, similar to TBOpt, while the GGA and meta-GGA hybrid DFAs give highly peaked distributions with a maximum near −0.7, which indicate water coordination via H-bonding, similar to TB.

"traditional" cavity models, such as the one-electron TB model,[30] which has a q_{cav} of essentially zero.

5. Hydrated electron–water coordination angular distributions

Although RDFs provide information on typical electron–water distances as well as coordination numbers, they do not directly give information on the orientations of the water molecules surrounding the e^-_{hyd}. Thus, we computed water dipole dot product distributions for every DFA that produced a localized e^-_{hyd}, as described in Sec. II. In brief, the dot product is taken between unit vectors connecting the hydrated electron's center of mass to the oxygen of a first-shell coordinating water molecule and that water's dipole vector. Dot products around −0.7 are characteristic of H-bond coordination.

Figure 3 shows the angular distributions of the first solvent-shell waters for each DFA that produced a localized e^-_{hyd}, as well as for the TB and TBOpt pseudopotential models. The data show that every model (except TBOpt) produces a peak near −0.7, indicating H-bond coordination to the hydrated electron. The TB and, particularly, TBOpt MQC models give relatively broad distributions, indicating that the first-shell waters have enhanced librational and rotational freedom. The DFT-based PBEh(25%; 40%) and R2SCANh(25%; 50%) e^-_{hyd} first-shell angular distributions, on the other hand, are sharply peaked, indicating that the first-shell water molecules are oriented to a significant degree. We have argued previously that this type of strong locking of the orientation of the first-shell waters is likely a result of charge delocalization error, as the electron can best mix into empty orbitals on the water molecules when they are in a particular geometry.[19]

In contrast, the LDA and LDAh(25%) DFAs show broader distributions of dot product values, characteristic of weaker solvent orientational ordering. Interestingly, the LDA-simulated e^-_{hyd} shows a preference for a distorted hydrogen-bond coordination, as the highest peak in its angular distribution occurs near −0.5. It is possible that this result is an artifact associated with the overestimation of the water–water H-bonding strength by the LDA functional.[57] The angular distribution of waters associated with the LDAh(25%) electron appears similar to that of the MQC models, where the librations of first-shell waters are much less restricted. Overall, along with the RDFs shown in Fig. 2, it appears that the e^-_{hyd}'s simulated with hybrid GGA and meta-GGA functionals orient first-shell water molecules more strongly than those produced via LDA, LDAh(25%), and the pseudopotential models. We note that the hydrated electron is known to have a large and positive solvation entropy,[58] indicating that this species is a champion chaotrope. Chaotropic ions are known to enhance the fluctuations of nearby solvent molecules,[23] so experiment suggests that the first-shell water molecules should have a broad angular distribution as opposed to a very narrow one, in contrast to those produced by most of the DFAs studied here.

6. Partial molar volume of DFT-simulated hydrated electrons

The partial molar volume (V_M) is a thermodynamic quantity that measures how much the volume of a solution changes when 1 mol of a particular solute is added. For the e^-_{hyd}, the partial molar volume is known experimentally to be 26 ± 6 cm^3/mol.[59,60] It has been shown from Kirkwood–Buff theory that V_M can be calculated from simulation as an integral over the electron–water radial distribution function;[18] this means that the entire solvation structure encoded in the RDF, not just the central cavity volume, impacts V_M. We note that the correct prediction of V_M does not necessarily validate an RDF as being experimentally correct, as there could be

many different RDFs that yield the same partial molar volume. However, an RDF that produces an incorrect V_M indicates a solvation structure that is assuredly not in agreement with experiment.

Table III shows values of V_M for each DFA that produces a localized e^-_{hyd}, along with those for the MQC models.[18,33] All the DFT-simulated hydrated electrons yield a V_M that drastically underestimates the magnitude of the experimental value (by a factor of ~3.5 to more than an order of magnitude), indicating that none of the RDFs produced by these simulations are correct. We note that the partial molar volumes computed for these DFAs are likely not converged with respect to the size of the simulation, as we have discussed in a previous study;[29] however, the numbers presented here for the DFT-simulated electrons are at least all computed at the same system size, so they can be compared directly to each other. PBEh(25%; 40%) produce the largest V_M values (a factor of ~3 underestimated from experiment), while the other DFAs that produce localized hydrated electrons have V_M's that are even more underestimated. The DFAs that yield non-localized electrons effectively have $V_M = 0$ since they do not perturb the water structure, again emphasizing their disagreement with experiment. Thus, other than the TB model, none of the simulations we explore in this work are able to correctly predict this important structural parameter.

C. Absorption spectroscopy of the DFT-simulated hydrated electron

The absorption spectrum of the hydrated electron has been well studied experimentally.[17,61] The line shape is Gaussian on the red side and Lorentzian on the blue side and is usually thought of as consisting of three strongly-allowed $s \rightarrow p$ transitions, as would arise from a particle-in-a-quasi-spherical-box model, plus a blue tail arising from weaker bound-to-continuum transitions.[4] Natural transition orbital (NTO) analyses of time-dependent density functional theory (TD-DFT) calculations have corroborated the $s \rightarrow p$ nature of the main transitions,[4] although most theoretical predictions of the spectrum do not properly capture the blue tail.[4,34]

In the literature, several different methods have been used to predict the absorption spectrum of the e^-_{hyd} simulated with DFT. Ambrosio *et al.*[62] estimated the absorption spectrum by binning the differences in Kohn–Sham orbital energies relative to the ground state from a fully periodic simulation with 64 waters using the PBEh(40%) XC functional. Although this attempt resulted in a spectrum that is in good agreement with experiment after a linear shift of the absorption spectrum maximum was applied, we have shown that if this same procedure is done using TD-DFT orbital energies, the resulting spectrum becomes overly blueshifted and highly structured, which is in stark disagreement with experiment.[25] Moreover, the use of periodic simulations that employ the Tamm–Dancoff approximation (TDA)[54] for TD-DFT produce spectra that do not follow the sum rules used in spectral moment analysis.[17]

More recently, Lan *et al.*[63] have used a quantum mechanics/molecular mechanics (QM/MM) approach, where configurations from a multi-time step (MTS) molecular dynamics simulation were fed into a non-periodic TD-DFT/MM absorption spectrum calculation using PBEh(40%). Although this non-periodic methodology should be superior to TDA TD-DFT, it is known that global hybrid functionals, such as PBEh, often produce spurious, low-lying charge transfer states.[64–66] These spurious states, commonly referred to as "ghost states," result in calculated absorption spectra that include excitations that are not physical. Some studies choose to simply neglect these states based on a radius of gyration criterion, but even with this approximation, the resulting spectra of the e^-_{hyd} are still blueshifted relative to experiment by nearly 0.5 eV.[62] We note that there are methods that have been developed explicitly to detect such spurious states,[66] although detecting and removing such states for every configuration in an ensemble is costly and laborious.

Uhlig *et al.*[15] have argued that the best way to calculate the e^-_{hyd}'s absorption spectrum is to extract configurations from periodic simulations, replicate them into a large, non-periodic supercell, and then calculate the spectrum using TD-DFT with an optimally-tuned range-separated hybrid functional. The use of a non-periodic calculation means that quantum mechanical spectral sum rules are satisfied and finite-size effects are minimized, and the use of an optimally-tuned range-separated hybrid functional[15] also eliminates spurious ghost states. In Secs. III C 1–III C 3, we will show that the hydrated electron's absorption spectrum is highly sensitive both to the methodology used as well as to the propagation functional. To date, regardless of the kind of methodology used to calculate the hydrated electron's absorption spectrum, DFT-based simulations have been unable to reproduce the position, width, shape, and degree of homogeneous broadening of the experimental spectrum.[19]

1. Fully periodic methodology

The simplest and most computationally inexpensive method for calculating the DFT-simulated e^-_{hyd} absorption spectrum in bulk water beyond simply binning the energy gaps between the Kohn–Sham orbitals[62] is by doing a periodic TDA TD-DFT calculation. Figure 4(a) shows the (normalized to the absorption maximum) spectra calculated using this methodology for each of the DFAs that produce a localized e^-_{hyd}, while Fig. 4(c) shows the spectra calculated for the PBE, R2SCAN, and REVTM DFAs that produce delocalized hydrated electrons. Here, the TD-DFT calculations were performed using the same functional that was used for propagating the e^-_{hyd} trajectory. Both panels also show the absorption spectra of the TB and TBOpt one-electron models (dashed curves), calculated by binning the transition dipoles between the one-electron ground and excited states, as well as the experimental spectrum (black curve).

Somewhat disturbingly, the XC functionals that produce delocalized hydrated electrons (PBE, R2SCAN, and REVTM) all predict spectra whose absorption maxima agree quite well with experiment [panel (c)]. It is likely that the large and non-physical blueshift induced by the periodic simulation methodology (discussed further below) coincidentally causes the DFAs that produce delocalized hydrated electrons to give spectra with reasonable E_{max} values. In other words, these spectra should be highly redshifted given their large R_g's,[4] but the unphysical blue shift induced by the periodic calculation happens to bring the spectra into apparent agreement with experiment.

All of the functionals that produce localized hydrated electrons [panel (a)] yield predicted absorption spectra that are substantially too blueshifted, with the lowest-level DFA, LDA, providing the best agreement with an E_{max} that is "only" ~0.75 eV off from the experimental value. The spectra also show an exaggerated blue shoulder, with PBEh(25%) having the least exaggerated blue shoulder of the XC functionals we tested. Adding more H–F

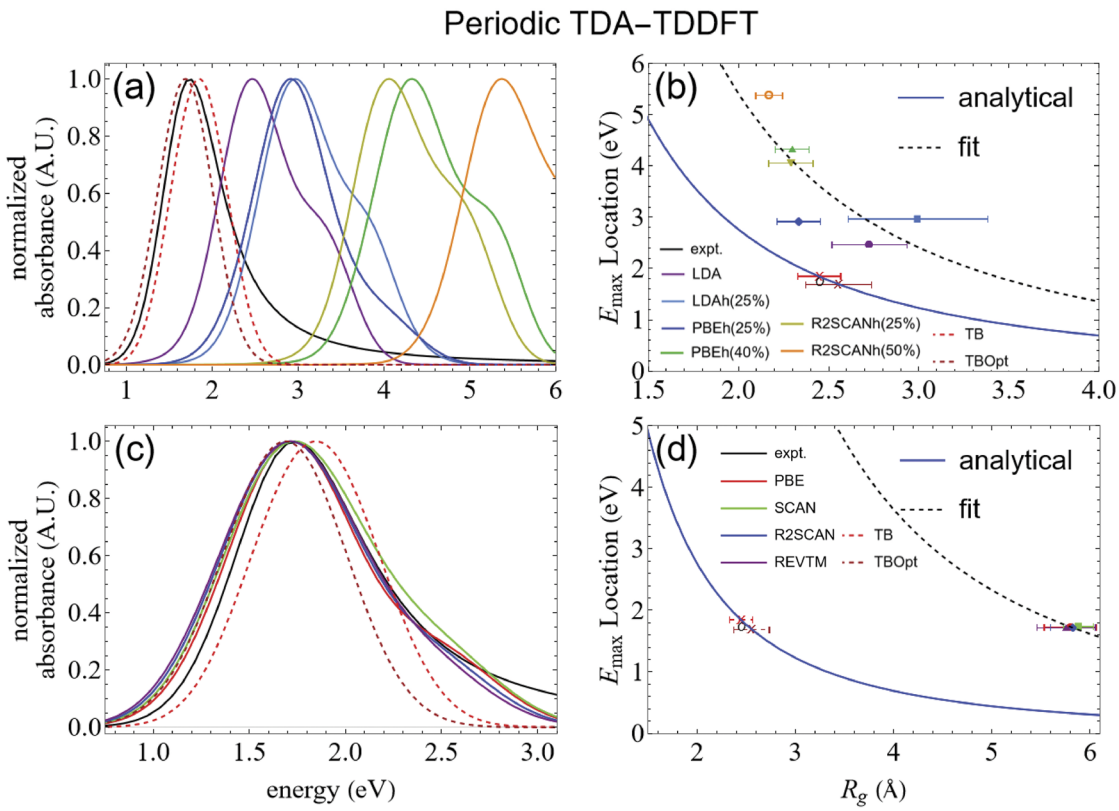

FIG. 4. Panels (a) and (c) show e^-_{hyd} absorption spectra calculated with fully periodic TDA TD-DFT using the same functional that was used to generate the hydrated electron configurations. This methodology results in a considerable blueshift of the E_{max}, which becomes even worse with the inclusion of H–F exchange. The DFAs that produce delocalized e^-_{hyd}'s [panel (c)] yield spectra that coincidentally match the experimental E_{max} well, a result due to the unphysical blue shift effect of the periodic cell. Panels (b) and (d) show the trend of E_{max} vs R_g^{-2} along with R_g^{-2} fits to the DFT-simulated spectra, as well as the analytical relationship from the particle-in-a-box approximation.[67] The DFAs that produce localized e^-_{hyd}'s qualitatively fit the expected relationship, although the data points lie well above the analytical curve. The DFAs that produce delocalized electrons do not follow the expected trend due to their spuriously large radii of gyration. We note that the radii of gyration were calculated from the periodic MD trajectories and not from the individual TDA TD-DFT calculations.

exchange to the hybrid functionals blueshifts the spectrum even more: LDAh(25%) and PBEh(25%) show similar highly blueshifted locations for their absorption maxima, while PBEh(40%) and R2SCANh(25%; 50%) are even further blueshifted. Although one might expect poor correspondence to the experimental spectra from periodic TDA TD-DFT calculations, it is still surprising that the hybrid meta-GGA functionals yield substantially worse spectral predictions than the hybrid GGAs with this methodology. The solvation structures produced by most of these DFAs are similar (cf. Figs. 2 and 3), so the primary factor in the varying spectral E_{max} values must stem from the inherent properties of each DFA rather than the solvation structures. This once again highlights the difficulty in predicting the accuracy of a given DFA, regardless of what rung of Jacob's Ladder[45] it comes from. The one-electron MQC models, in contrast, give quite a good match to the experimental E_{max}.

If one assumes that hydrated electrons can be crudely modeled as particles in a spherical box, electrons with large radii of gyration should produce redshifted spectra relative to more tightly-confined electrons, with an absorption maximum that varies inversely with the square of the cavity radius, as shown by the blue curves in Figs. 4(b) and 4(d). Indeed, the particle-in-a-spherical-box correspondence appears to hold somewhat well for the DFAs that produce localized e^-_{hyd}'s, although the fit curve lies well above the analytical curve due to the aforementioned unphysical blueshift. Conversely, the functionals that produce delocalized hydrated electrons do not follow this trend due to their spuriously large radii of gyration [Fig. 4(d)]. These results highlight the facts that (1) periodic calculations do not obey the quantum mechanical sum-rules and, thus, do not capture the correct relationship between the calculated spectral E_{max} and R_g and that (2) periodic calculations of e^-_{hyd} spectroscopy induce very large spectral blue shifts that worsen with increased H–F exchange percent. Since the periodic calculations use the same number of waters as the MD simulations (64 quantum mechanical waters), much of this spectral blueshift may result from finite size effects.

2. Non-periodic methodology

A more time-consuming and computationally expensive way to calculate spectra for the e^-_{hyd} is using non-periodic TD-DFT

with an optimally-tuned long-range corrected (LRC) functional.[15] Figure 5(a) shows the normalized spectra calculated this way for the functionals we tested that produce localized hydrated electrons, while panel (c) shows the same for the functionals that produce delocalized hydrated electrons. Here, we see that the hybrid functionals [with the exception of LDAh(25%), discussed below] produce spectra that are much more similar than those calculated using the periodic TDA TD-DFT method, which is better reflective of their similar solvation structures. The predicted spectra are also less blueshifted than in Fig. 4. The spectra computed for the LDA, PBEh(25% and 40%), and R2SCANh(25% and 50%) electrons all show red shoulders, which result from unphysical transitions between the central cavity and the surface of the periodically replicated water box.

Interestingly, both REVTM (purple curve), which produces a delocalized hydrated electron in the periodic calculation, and LDAh(25%) (blue curve) yield non-periodic TD-DFT spectra calculated with ωPBE that are very redshifted relative to experiment [Fig. 6(c)], characteristic of having far too large a radius of gyration. Both functionals also show a highly exaggerated blue shoulder that gives them a qualitatively incorrect spectral shape. The reason for the spectral similarity between these two DFAs is that the localized e^-_{hyd} configurations generated with LDAh(25%) yield a delocalized hydrated electron when calculated with the long-range corrected ωPBE functional used for the TD-DFT spectral calculation. This highlights an interesting difficulty in using the non-periodic TD-DFT methodology outlined by Uhlig *et al.*:[15] unexpected results can occur if the functional used to generate the configurations differs substantially from the range-separated hybrid functional used to calculate the spectroscopy.

Despite the fact that the mismatch between the DFAs used for trajectory production and spectroscopy can lead to difficulties, Fig. 5(b) shows that the dependence of E_{max} on the e^-_{hyd} radius of gyration holds quite well for the non-periodic TD-DFT calculations. We note that this methodology removes the explicit finite size effects present in the periodic absorption spectra calculations, although there still could be implicit finite size effects present in the configurations generated by running the original MD trajectories using only 64 water molecules. However, in previous studies with

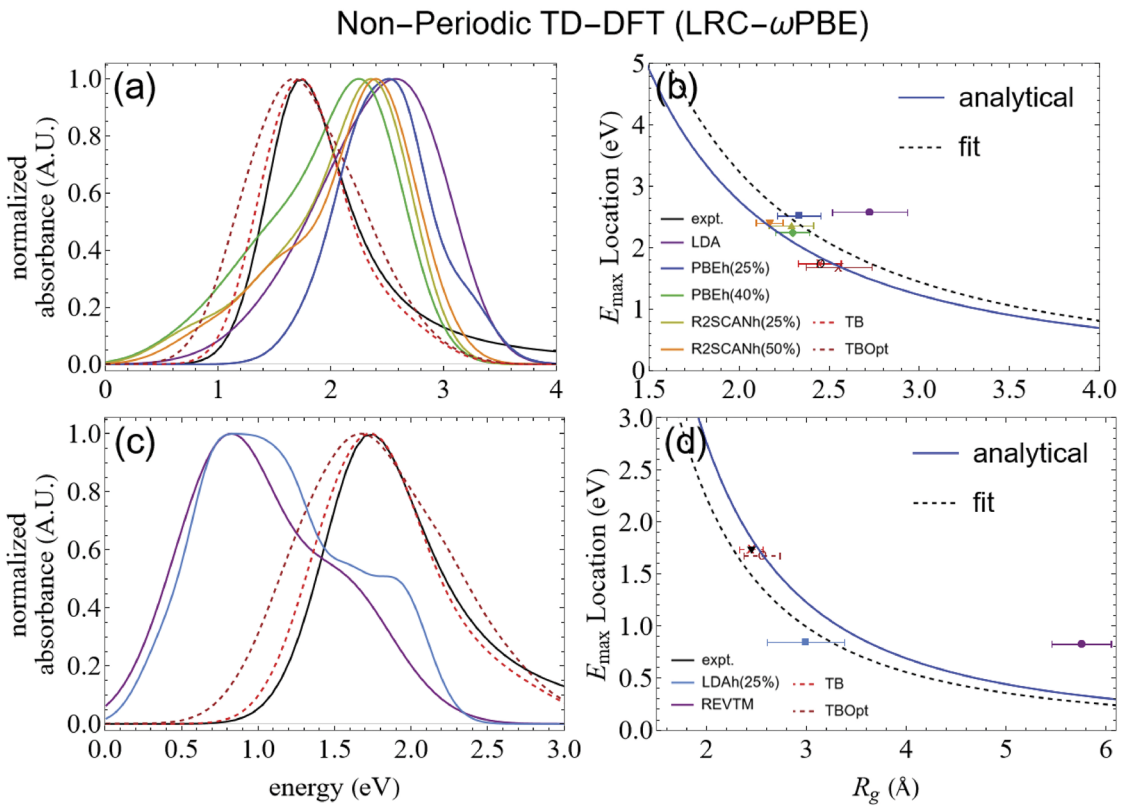

FIG. 5. Hydrated electron absorption spectra calculated using non-periodic TD-DFT with the optimally-tuned LRC-ωPBE functional with periodic unit cell replication [panels (a) and (c)]. The spectral E_{max} vs R_g^{-2} fits (dashed black curves), along with the analytical relationship from particle in a spherical box theory (blue curves), are shown in panels (b) and (d). This non-periodic methodology avoids the unphysical blue shift induced by the periodic calculation seen in Fig. 4 as well as inhibits spurious charge transfer states.[66] The functionals that produce localized e^-_{hyd}'s [panels (a) and (b)] give E_{max} values that are still a few hundred meV blue shifted relative to the experimental spectrum; they also exhibit a tail to the red that is qualitatively different from the experimental spectral shape (black curve). With this non-periodic methodology, the expected E_{max} vs R_g^{-2} trend is followed quite well (dashed black curve), almost matching the analytical result (blue curve). The functionals that produce delocalized hydrated electrons [panels (c) and (d)] predict strongly red-shifted spectra relative to experiment, although they do show a reasonable fit to the E_{max} vs R_g^{-2} trend. We note that radii of gyration values plotted in panels (b) and (d) are those obtained from the periodic simulations, not the non-periodic TD-DFT calculations.

the PBEh(25%) functional and different-sized simulation boxes, we showed that this type of implicit finite size effect is modest.[25] We also used non-periodic TD-DFT calculations with LRC-ωPBE to calculate the spectroscopy for configurations generated from the TB and TBOpt pseudopotentials and find that these not only match the experimental spectrum well but also fall directly on the analytical E_{max} vs R_g^{-2} curve [Figs. 5(b) and 5(d)], in agreement with previous studies.[68,69] This suggests that a softer cavity structure, such as those generated by the one-electron calculations or the LDAh(25%) DFA, is closer to experiment than the harder cavity structures predicted by effectively all of the other XC functionals that we tested.

3. Vertical binding energy (VBE)

The vertical binding energy (VBE) is another experimentally verifiable measure of the e^-_{hyd} electronic structure. However, computing this observable from periodic TD-DFT simulations is challenging given the difficulty in defining a rigorous vacuum level to which the computed VBE can be compared.[62] One advantage of running non-periodic TD-DFT calculations with unit cell replication for the above spectral analyses is that these calculations also directly yield a well-defined VBE relative to vacuum. Table II shows the VBE values obtained from our non-periodic calculations for each XC functional we used that produce a localized e^-_{hyd}, as well as experiment. It is clear that all of the DFAs underestimate the VBE by a factor of about 2. With increasing amounts of H–F exchange, we see opposite trends in the VBE for the PBEh and R2SCANh DFAs, highlighting once again that tuning H–F exchange can have unexpected impacts on quantities related to the electronic structure.[44] We note that the VBE is quite sensitive to finite size effects as well as the tuning of the long-range correction parameter, as we have shown in previous studies.[25] It is, therefore, possible that larger system sizes and/or further functional-dependent tuning of the range-separation parameter could bring these VBE values into better agreement with experiment.

IV. CONCLUSIONS

This work has presented a series of *ab initio* DFT simulations of the hydrated electron using a variety of DFAs spanning Jacob's Ladder.[45] We simulated the e^-_{hyd} using several functionals that, to our knowledge, have never been previously applied to this system. We calculated many of the hydrated electron's observables, including those that pertain to the electron's size and shape (R_g, asphericity, and q_{cav}), hydration structure (RDFs, coordination numbers, angular distributions, charge distributions, and partial molar volume), energetics (VBEs), and spectroscopy (absorption spectra). We also compared two common methodologies for calculating hydrated electron spectroscopy: fully-periodic TDA TD-DFT calculated with the same functional used to simulate the e^-_{hyd} and non-periodic TDDFT with point-charge water replication using an optimally-tuned range-separated hybrid functional.

We found first that not all XC functionals produce a localized e^-_{hyd}, with most of the non-hybrid functionals and also the SCANh DFA yielding a delocalized (or chemically reacted) charge distribution. This emphasizes the fact that DFT is not a systematically improvable theory, particularly given all of the challenges with using DFT to describe both liquid water and the excess electron that lies primarily between the waters.[42] Interestingly, of the DFAs that produce a localized e^-_{hyd}, the radius of gyration and solvation structure measures (RDFs, coordination numbers, angular distributions, asphericity, q_{cav}, and charge distributions) are largely similar within the uncertainty, suggesting that most equilibrium properties are not significantly changed moving from the LDA functional up to hybrid meta-GGAs. Increasing the amount of H–F exchange generally acts to further localize the hydrated electron into its central cavity, reducing donation of charge onto surrounding water molecules.

Spectra of the e^-_{hyd} calculated using periodic TDA TD-DFT are significantly blueshifted (≥1 eV except for LDA) relative to experiment; the spectra calculated this way also do not follow the expected relationship between the position of the spectral maximum and the electron's radius of gyration. The grossly exaggerated blueshift is partly remedied by using a more expensive non-periodic calculation with an optimally-tuned range-separated hybrid functional and periodic replication of point-charge water molecules. When the non-periodic method is used, the hybrid meta-GGA functional R2SCANh DFAs yield the best E_{max} relative to experiment (although still off by hundreds of meV), and the expected trend of E_{max} vs R_g^{-2} holds quite well.

It is worth noting that for all of the observables we calculated, no particular functional stands out as markedly better than the others for predicting any single observable of the e^-_{hyd}. This means that when considering the increased computational cost associated with using hybrid meta-GGA DFAs, the use of less expensive functionals is actually a reasonable choice if one wishes to simulate hydrated electrons at the DFT level of theory; for example, the LDA functional performs far better than expected, not only producing a localized e^-_{hyd} but one with observables that are within error the same as those produced by much higher level functionals for a much lower computational cost.

We close by noting that none of the DFAs we tested produce the correct partial molar volume of the e^-_{hyd} to within a factor of ~3, correctly predict the shape of the absorption spectrum or E_{max} value to within 1 eV, or predict the correct VBE value to within a factor of ~2. Moreover, the equilibrium hydration structure (characterized by sharply peaked RDFs and angular distributions) is not qualitatively consistent with what is expected for a chaotropic ion, in contradiction with the large positive solvation entropy measured for this species.[58] Given this, it is unlikely that any of the DFAs explored here reproduce the correct structure and dynamics of water molecules near the electron. Although finite size effects may explain some of these disagreements with experiment, our work using the PBEh(25%) functional showed that such effects were modest for most observables.[25,29] In future work, we plan to focus on density-corrected DFT[70] (DC-DFT) as well as propagation with optimally tuned range-separated hybrid functionals. If SIE is the dominant factor in the errors DFT makes on hydrated electron systems, DC-DFT should markedly attenuate those density-driven errors. It has been shown that range-separated hybrid functionals can greatly impact the ion-pairing behavior in DFT-based simulations,[71] so range-separated DFAs could be crucial in modulating a given ion's kosmotropic/chaotropic character. Finally, including explicit nuclear quantum effects (NQEs) in hydrated electron simulations is a worthwhile endeavor that has only begun to be studied,[14,40] as it is possible that including quantum delocalization for water molecules

would destructure the first solvation shell, increasing the chaotropic character of the e^-_{hyd}.

ACKNOWLEDGMENTS

This work was supported by the National Science Foundation, under Grant No. CHE-2247583. Partial support for W.R.B. was provided by the U.S. Department of Energy, Basic Energy Sciences Condensed-Phase and Interfacial Molecular Science Program, under Grant No. DE-SC0017800. Computational resources were provided by the University of California, Los Angeles (UCLA), Institute for Digital Research and Education, and Extreme Science and Engineering Discovery Environment (XSEDE), under Computational Project No. TG-CHE170065.

AUTHOR DECLARATIONS

Conflict of Interest

The authors have no conflicts to disclose.

Author Contributions

William R. Borrelli: Conceptualization (equal); Data curation (lead); Formal analysis (lead); Methodology (lead); Resources (lead); Software (lead); Validation (lead); Visualization (equal); Writing – original draft (lead); Writing – review & editing (equal). **Xiaoyan Liu**: Data curation (supporting); Methodology (supporting). **Benjamin J. Schwartz**: Conceptualization (equal); Funding acquisition (lead); Project administration (lead); Supervision (lead); Visualization (equal); Writing – review & editing (equal).

DATA AVAILABILITY

Trajectory files for simulations with the functionals that produced localized hydrated electrons are in a Dryad repository (https://doi.org/10.5061/dryad.gmsbcc2zd), which is freely accessible. The repository contains XYZ formatted files of the AIMD trajectories simulated with each functional that produced a localized hydrated electron. Trajectories are given over the equilibrated regime of each simulation.

REFERENCES

[1] S. Gordon, E. J. Hart, M. S. Matheson, J. Rabani, and J. K. Thomas, "Reactions of the hydrated electron," Discuss. Faraday Soc. **36**, 193–205 (1963).
[2] E. J. Hart, "The hydrated electron," Science **146**, 19–25 (1964).
[3] T. W. Marin, K. Takahashi, C. D. Jonah, S. D. Chemerisov, and D. M. Bartels, "Recombination of the hydrated electron at high temperature and pressure in hydrogenated alkaline water," J. Phys. Chem. A **111**, 11540–11551 (2007).
[4] J. M. Herbert and M. P. Coons, "The hydrated electron," Annu. Rev. Phys. Chem. **68**, 447–472 (2017).
[5] A. Kumar, D. Becker, A. Adhikary, and M. D. Sevilla, "Reaction of electrons with DNA: Radiation damage to radiosensitization," Int. J. Mol. Sci. **20**, 3998 (2019).
[6] P. Neupane, D. M. Bartels, and W. H. Thompson, "Exploring the unusual reactivity of the hydrated electron with CO_2," J. Phys. Chem. B **128**, 567–575 (2024).
[7] R. Daily and D. Minakata, "Reactivities of hydrated electrons with organic compounds in aqueous-phase advanced reduction processes," Environ. Sci.: Water Res. Technol. **8**, 543–574 (2022).
[8] N. Basco, G. A. Kenney-Wallace, S. K. Vidyarthi, and D. C. Walker, "A transient intermediate in the bimolecular reaction of hydrated electrons," Can. J. Chem. **50**, 2059–2070 (1972).
[9] W. R. Borrelli, J. L. Guardado Sandoval, K. J. Mei, and B. J. Schwartz, "Roles of H-bonding and hydride solvation in the reaction of hydrated (Di)electrons with water to create H_2 and OH^-," J. Chem. Theory Comput. **20**, 7337 (2024).
[10] T. L. Huyen, T. V. Pham, M. T. Nguyen, and M. C. Lin, "A model study on the mechanism and kinetics for reactions of the hydrated electron with H_3O^+ and NH_4^+ ions," Chem. Phys. Lett. **731**, 136604 (2019).
[11] B. D. Fennell, D. Fowler, S. P. Mezyk, and G. McKay, "Reactivity of dissolved organic matter with the hydrated electron: Implications for treatment of chemical contaminants in water with advanced reduction processes," Environ. Sci. Technol. **57**, 7634–7643 (2023).
[12] V. V. Rybkin, "Mechanism of aqueous carbon dioxide reduction by the solvated electron," J. Phys. Chem. B **124**, 10435–10441 (2020).
[13] C. J. Jordan, M. P. Coons, J. M. Herbert, and J. R. Verlet, "Spectroscopy and dynamics of the hydrated electron at the water/air interface," Nat. Commun. **15**, 182 (2024).
[14] F. Novelli, K. Chen, A. Buchmann, T. Ockelmann, C. Hoberg, T. Head-Gordon, and M. Havenith, "The birth and evolution of solvated electrons in the water," Proc. Natl. Acad. Sci. U. S. A. **120**, e2216480120 (2023).
[15] F. Uhlig, J. M. Herbert, M. P. Coons, and P. Jungwirth, "Optical spectroscopy of the bulk and interfacial hydrated electron from ab initio calculations," J. Phys. Chem. A **118**, 7507–7515 (2014).
[16] P. Neupane, A. Katiyar, D. M. Bartels, and W. H. Thompson, "Investigation of the failure of Marcus theory for hydrated electron reactions," J. Phys. Chem. Lett. **13**, 8971–8977 (2022).
[17] D. M. Bartels, "Moment analysis of hydrated electron cluster spectra: Surface or internal states?," J. Chem. Phys. **115**, 4404–4405 (2001).
[18] P. Neupane, D. M. Bartels, and W. H. Thompson, "Relation between the hydrated electron solvation structure and its partial molar volume," J. Phys. Chem. B **127**, 5941 (2023).
[19] S. J. Park and B. J. Schwartz, "How ions break local symmetry: Simulations of polarized transient hole burning for different models of the hydrated electron in contact pairs with Na^+," J. Phys. Chem. Lett. **14**, 3014–3022 (2023).
[20] H. Y. Liu, K. J. Mei, W. R. Borrelli, and B. J. Schwartz, "Simulating the competitive ion pairing of hydrated electrons with chaotropic cations," J. Phys. Chem. B **128**, 8557–8566 (2024).
[21] W. A. Narvaez, S. J. Park, and B. J. Schwartz, "Competitive ion pairing and the role of anions in the behavior of hydrated electrons in electrolytes," J. Phys. Chem. B **126**, 7701–7708 (2022).
[22] S. J. Park, W. A. Narvaez, and B. J. Schwartz, "How water–ion interactions control the formation of hydrated electron: Sodium cation contact pairs," J. Phys. Chem. B **125**, 13027–13040 (2021).
[23] K. D. Collins, "Charge density-dependent strength of hydration and biological structure," Biophys. J. **72**, 65–76 (1997).
[24] S. J. Park, W. A. Narvaez, and B. J. Schwartz, "Ab initio studies of hydrated electron/cation contact pairs: Hydrated electrons simulated with density functional theory are too kosmotropic," J. Phys. Chem. Lett. **14**, 559–566 (2023).
[25] S. J. Park and B. J. Schwartz, "Understanding the temperature dependence and finite size effects in *ab initio* MD simulations of the hydrated electron," J. Chem. Theory Comput. **18**, 4973–4982 (2022).
[26] F. Uhlig, O. Marsalek, and P. Jungwirth, "Unraveling the complex nature of the hydrated electron," J. Phys. Chem. Lett. **3**, 3071–3075 (2012).
[27] O. Marsalek, F. Uhlig, J. VandeVondele, and P. Jungwirth, "Structure, dynamics, and reactivity of hydrated electrons by ab initio molecular dynamics," Acc. Chem. Res. **45**, 23–32 (2012).
[28] M. Pizzochero, F. Ambrosio, and A. Pasquarello, "Picture of the wet electron: A localized transient state in liquid water," Chem. Sci. **10**, 7442–7448 (2019).
[29] W. R. Borrelli, K. J. Mei, S. J. Park, and B. J. Schwartz, "Partial molar solvation volume of the hydrated electron simulated via DFT," J. Phys. Chem. B **128**, 2425–2431 (2024).
[30] L. Turi and D. Borgis, "Analytical investigations of an electron–water molecule pseudopotential. II. Development of a new pair potential and molecular dynamics simulations," J. Chem. Phys. **117**, 6186–6195 (2002).

[31]W. J. Glover and B. J. Schwartz, "Short-range electron correlation stabilizes noncavity solvation of the hydrated electron," J. Chem. Theory Comput. **12**, 5117–5131 (2016).
[32]R. E. Larsen, W. J. Glover, and B. J. Schwartz, "Does the hydrated electron occupy a cavity?," Science **329**, 65–69 (2010).
[33]P. Neupane, D. M. Bartels, and W. H. Thompson, "Empirically optimized one-electron pseudopotential for the hydrated electron: A proof-of-concept study," J. Phys. Chem. B **127**, 7361–7371 (2023).
[34]P. J. Rossky and J. Schnitker, "The hydrated electron: Quantum simulation of structure, spectroscopy, and dynamics," J. Phys. Chem. **92**, 4277–4285 (1988).
[35]W. J. Glover, R. E. Larsen, and B. J. Schwartz, "First principles multielectron mixed quantum/classical simulations in the condensed phase. I. An efficient Fourier-grid method for solving the many-electron problem," J. Chem. Phys. **132**, 144101 (2010).
[36]J. C. Phillips and L. Kleinman, "New method for calculating wave functions in crystals and molecules," Phys. Rev. **116**, 287–294 (1959).
[37]C.-C. Zho, E. P. Farr, W. J. Glover, and B. J. Schwartz, "Temperature dependence of the hydrated electron's excited-state relaxation. I. Simulation predictions of resonance Raman and pump-probe transient absorption spectra of cavity and non-cavity models," J. Chem. Phys. **147**, 074503 (2017).
[38]J. R. Casey, R. E. Larsen, and B. J. Schwartz, "Resonance Raman and temperature-dependent electronic absorption spectra of cavity and noncavity models of the hydrated electron," Proc. Natl. Acad. Sci. U. S. A. **110**, 2712–2717 (2013).
[39]C.-C. Zho and B. J. Schwartz, "Time-resolved photoelectron spectroscopy of the hydrated electron: Comparing cavity and noncavity models to experiment," J. Phys. Chem. B **120**, 12604–12614 (2016).
[40]J. Lan, V. Kapil, P. Gasparotto, M. Ceriotti, M. Iannuzzi, and V. V. Rybkin, "Simulating the ghost: Quantum dynamics of the solvated electron," Nat. Commun. **12**, 766 (2021).
[41]R. Gao, Y. Li, and R. Car, "Enhanced deep potential model for fast and accurate molecular dynamics: Application to the hydrated electron," Phys. Chem. Chem. Phys. **26**, 23080–23088 (2024).
[42]E. R. Johnson, A. Otero-de-la Roza, and S. G. Dale, "Extreme density-driven delocalization error for a model solvated-electron system," J. Chem. Phys. **139**, 184116 (2013).
[43]M. J. Gillan, D. Alfè, and A. Michaelides, "Perspective: How good is DFT for water?," J. Chem. Phys. **144**, 130901 (2016).
[44]E. Lambros, J. Hu, and F. Paesani, "Assessing the accuracy of the SCAN functional for water through a many-body analysis of the adiabatic connection formula," J. Chem. Theory Comput. **17**, 3739–3749 (2021).
[45]J. P. Perdew and K. Schmidt, "Jacob's ladder of density functional approximations for the exchange-correlation energy," AIP Conf. Proc. **577**, 1–20 (2001).
[46]T. D. Kühne, M. Iannuzzi, M. Del Ben, V. V. Rybkin, P. Seewald, F. Stein, T. Laino, R. Z. Khaliullin, O. Schütt, F. Schiffmann, D. Golze, J. Wilhelm, S. Chulkov, M. H. Bani-Hashemian, V. Weber, U. Borštnik, M. Taillefumier, A. S. Jakobovits, A. Lazzaro, H. Pabst, T. Müller, R. Schade, M. Guidon, S. Andermatt, N. Holmberg, G. K. Schenter, A. Hehn, A. Bussy, F. Belleflamme, G. Tabacchi, A. Glöß, M. Lass, I. Bethune, C. J. Mundy, C. Plessl, M. Watkins, J. VandeVondele, M. Krack, and J. Hutter, "CP2K: An electronic structure and molecular dynamics software package–Quickstep: Efficient and accurate electronic structure calculations," J. Chem. Phys. **152**, 194103 (2020).
[47]S. Grimme, J. Antony, S. Ehrlich, and H. Krieg, "A consistent and accurate *ab initio* parametrization of density functional dispersion correction (DFT-D) for the 94 elements H-Pu," J. Chem. Phys. **132**, 154104 (2010).
[48]K. J. Mei, W. R. Borrelli, J. L. Guardado Sandoval, and B. J. Schwartz, "How to probe hydrated dielectrons experimentally: *Ab initio* simulations of the absorption spectra of aqueous dielectrons, electron pairs, and hydride," J. Phys. Chem. Lett. **15**, 9557–9565 (2024).
[49]W. A. Narvaez, E. C. Wu, S. J. Park, M. Gomez, and B. J. Schwartz, "Trap-seeking or trap-digging? Photoinjection of hydrated electrons into aqueous NaCl solutions," J. Phys. Chem. Lett. **13**, 8653–8659 (2022).
[50]S. Goedecker, M. Teter, and J. Hutter, "Separable dual-space Gaussian pseudopotentials," Phys. Rev. B **54**, 1703–1710 (1996).
[51]M. Guidon, J. Hutter, and J. VandeVondele, "Auxiliary density matrix methods for Hartree–Fock exchange calculations," J. Chem. Theory Comput. **6**, 2348–2364 (2010).
[52]G. J. Martyna, M. L. Klein, and M. Tuckerman, "Nosé–Hoover chains: The canonical ensemble via continuous dynamics," J. Chem. Phys. **97**, 2635–2643 (1992).
[53]S. J. Park and B. J. Schwartz, "Evaluating simple *ab initio* models of the hydrated electron: The role of dynamical fluctuations," J. Phys. Chem. B **124**, 9592–9603 (2020).
[54]S. Hirata and M. Head-Gordon, "Time-dependent density functional theory within the Tamm–Dancoff approximation," Chem. Phys. Lett. **314**, 291–299 (1999).
[55]E. Epifanovsky, A. T. B. Gilbert, X. Feng, J. Lee, Y. Mao, N. Mardirossian, P. Pokhilko, A. F. White, M. P. Coons, A. L. Dempwolff, Z. Gan, D. Hait, P. R. Horn, L. D. Jacobson, I. Kaliman, J. Kussmann, A. W. Lange, K. U. Lao, D. S. Levine, J. Liu, S. C. McKenzie, A. F. Morrison, K. D. Nanda, F. Plasser, D. R. Rehn, M. L. Vidal, Z.-Q. You, Y. Zhu, B. Alam, B. J. Albrecht, A. Aldossary, E. Alguire, J. H. Andersen, V. Athavale, D. Barton, K. Begam, A. Behn, N. Bellonzi, Y. A. Bernard, E. J. Berquist, H. G. A. Burton, A. Carreras, K. Carter-Fenk, R. Chakraborty, A. D. Chien, K. D. Closser, V. Cofer-Shabica, S. Dasgupta, M. de Wergifosse, J. Deng, M. Diedenhofen, H. Do, S. Ehlert, P.-T. Fang, S. Fatehi, Q. Feng, T. Friedhoff, J. Gayvert, Q. Ge, G. Gidofalvi, M. Goldey, J. Gomes, C. E. González-Espinoza, S. Gulania, A. O. Gunina, M. W. D. Hanson-Heine, P. H. P. Harbach, A. Hauser, M. F. Herbst, M. Hernández Vera, M. Hodecker, Z. C. Holden, S. Houck, X. Huang, K. Hui, B. C. Huynh, M. Ivanov, Á. Jász, H. Ji, H. Jiang, B. Kaduk, S. Kähler, K. Khistyaev, J. Kim, G. Kis, P. Klunzinger, Z. Koczor-Benda, J. H. Koh, D. Kosenkov, L. Koulias, T. Kowalczyk, C. M. Krauter, K. Kue, A. Kunitsa, T. Kus, I. Ladjánszki, A. Landau, K. V. Lawler, D. Lefrancois, S. Lehtola, R. R. Li, Y.-P. Li, J. Liang, M. Liebenthal, H.-H. Lin, Y.-S. Lin, F. Liu, K.-Y. Liu, M. Loipersberger, A. Luenser, A. Manjanath, P. Manohar, E. Mansoor, S. F. Manzer, S.-P. Mao, A. V. Marenich, T. Markovich, S. Mason, S. A. Maurer, P. F. McLaughlin, M. F. S. J. Menger, J.-M. Mewes, S. A. Mewes, P. Morgante, J. W. Mullinax, K. J. Oosterbaan, G. Paran, A. C. Paul, S. K. Paul, F. Pavošević, Z. Pei, S. Prager, E. I. Proynov, Á. Rák, E. Ramos-Cordoba, B. Rana, A. E. Rask, A. Rettig, R. M. Richard, F. Rob, E. Rossomme, T. Scheele, M. Scheurer, M. Schneider, N. Sergueev, S. M. Sharada, W. Skomorowski, D. W. Small, C. J. Stein, Y.-C. Su, E. J. Sundstrom, Z. Tao, J. Thirman, G. J. Tornai, T. Tsuchimochi, N. M. Tubman, S. P. Veccham, O. Vydrov, J. Wenzel, J. Witte, A. Yamada, K. Yao, S. Yeganeh, S. R. Yost, A. Zech, I. Y. Zhang, X. Zhang, Y. Zhang, D. Zuev, A. Aspuru-Guzik, A. T. Bell, N. A. Besley, K. B. Bravaya, B. R. Brooks, D. Casanova, J.-D. Chai, S. Coriani, C. J. Cramer, G. Cserey, A. E. DePrince III, R. A. DiStasio, Jr., A. Dreuw, B. D. Dunietz, T. R. Furlani, W. A. Goddard III, S. Hammes-Schiffer, T. Head-Gordon, W. J. Hehre, C.-P. Hsu, T.-C. Jagau, Y. Jung, A. Klamt, J. Kong, D. S. Lambrecht, W. Liang, N. J. Mayhall, C. W. McCurdy, J. B. Neaton, C. Ochsenfeld, J. A. Parkhill, R. Peverati, V. A. Rassolov, Y. Shao, L. V. Slipchenko, T. Stauch, R. P. Steele, J. E. Subotnik, A. J. W. Thom, A. Tkatchenko, D. G. Truhlar, T. Van Voorhis, T. A. Wesolowski, K. B. Whaley, H. L. Woodcock III, P. M. Zimmerman, S. Faraji, P. M. W. Gill, M. Head-Gordon, J. M. Herbert, and A. I. Krylov, "Software for the frontiers of quantum chemistry: An overview of developments in the Q-Chem 5 package," J. Chem. Phys. **155**, 084801 (2021).
[56]W. R. Borrelli, X. Liu, and B. J. Schwartz, "Evaluating the chemical reactivity of DFT-simulated liquid water with hydrated electrons via the dual descriptor," J. Chem. Theory Comput. **20**, 9571 (2024).
[57]M. Chen, H.-Y. Ko, R. C. Remsing, M. F. Calegari Andrade, B. Santra, Z. Sun, A. Selloni, R. Car, M. L. Klein, J. P. Perdew, and X. Wu, "Ab initio theory and modeling of water," Proc. Natl. Acad. Sci. U. S. A. **114**, 10846–10851 (2017).
[58]P. Han and D. M. Bartels, "On the hydrated electron as a structure-breaking ion," J. Phys. Chem. **95**, 5367–5370 (1991).
[59]I. Janik, A. Lisovskaya, and D. M. Bartels, "Partial molar volume of the hydrated electron," J. Phys. Chem. Lett. **10**, 2220–2226 (2019).
[60]C. D. Borsarelli, S. G. Bertolotti, and C. M. Previtali, "Thermodynamic changes associated with the formation of the hydrated electron after photoionization of inorganic anions: A time-resolved photoacoustic study," Photochem. Photobiol. Sci. **2**, 791–795 (2003).
[61]E. J. Hart and J. W. Boag, "Absorption spectrum of the hydrated electron in water and in aqueous solutions," J. Am. Chem. Soc. **84**, 4090–4095 (1962).

[62] F. Ambrosio, G. Miceli, and A. Pasquarello, "Electronic levels of excess electrons in liquid water," J. Phys. Chem. Lett. **8**, 2055–2059 (2017).
[63] J. Lan, V. V. Rybkin, and A. Pasquarello, "Temperature dependent properties of the aqueous electron," Angew. Chem., Int. Ed. **61**, e202209398 (2022).
[64] A. Dreuw, J. L. Weisman, and M. Head-Gordon, "Long-range charge-transfer excited states in time-dependent density functional theory require non-local exchange," J. Chem. Phys. **119**, 2943–2946 (2003).
[65] A. Dreuw and M. Head-Gordon, "Failure of time-dependent density functional theory for long-range charge-transfer excited states: The zincbacteriochlorin–bacteriochlorin and bacteriochlorophyll–spheroidene complexes," J. Am. Chem. Soc. **126**, 4007–4016 (2004).
[66] M. Campetella, F. Maschietto, M. J. Frisch, G. Scalmani, I. Ciofini, and C. Adamo, "Charge transfer excitations in TDDFT: A ghost-hunter index," J. Comput. Chem. **38**, 2151–2156 (2017).
[67] D.-F. Feng and L. Kevan, "Theoretical models for solvated electrons," Chem. Rev. **80**, 1–20 (1980).
[68] J. M. Herbert and L. D. Jacobson, "Structure of the aqueous electron: Assessment of one-electron pseudopotential models in comparison to experimental data and time-dependent density functional theory," J. Phys. Chem. A **115**, 14470–14483 (2011).
[69] L. Turi, B. Baranyi, and Á. Madarász, "2-in-1 phase space sampling for calculating the absorption spectrum of the hydrated electron," J. Chem. Theory Comput. **20**, 4265–4277 (2024).
[70] S. Song, S. Vuckovic, E. Sim, and K. Burke, "Density-corrected DFT explained: Questions and answers," J. Chem. Theory Comput. **18**, 817–827 (2022).
[71] Y. Yao and Y. Kanai, "Free energy profile of NaCl in water: First-principles molecular dynamics with SCAN and ωB97X-V exchange–correlation functionals," J. Chem. Theory Comput. **14**, 884–893 (2018).